RSC Advances

PAPER

View Article Online
View Journal | View Issue

Cite this: *RSC Adv.*, 2021, **11**, 20081

A conductive polymer composed of a cellulose-based flexible film and carbon nanotubes

Lechen Yang, [ab] Yan Wu, *[ab] Feng Yang*[c] and Wenhao Wang[ab]

Received 4th May 2021
Accepted 31st May 2021

DOI: 10.1039/d1ra03474j

rsc.li/rsc-advances

As a natural biological material, wood has renewability, biocompatibility, biodegradability and excellent mechanical properties. This research shows a conductive polymer composed of a cellulose-based flexible film constructed from natural wood and carbon nanotubes. Part of the lignin/hemicellulose of the natural wood was removed by the deep eutectic solvent to obtain a cellulose-based flexible film with a porous structure, and then the carbon nanotubes were infiltrated into the cellulose-based flexible film by vacuum pressure impregnation treatment to obtain the final conductive polymer. This conductive polymer has high conductivity and good toughness, and shows good perception ability under a certain range of strain/stress or human activity conditions. In addition, conductive fibers can be prepared by cutting and twisting the oriented cellulose nanofibers of this conductive polymer. The above-mentioned properties of this conductive polymer provide great potential for its development in electrical-related fields.

1. Introduction

Natural biomaterials have renewability, biocompatibility, biodegradability and excellent mechanical properties, as well as multiple reaction sites that modulate novel functions, so they possess outstanding advantages in high-performance and functional electronic devices.[1–3] In recent years, the application of natural biomaterials in flexible electronic devices has become a research hotspot. Natural biomaterials with good structures and forms (such as silk fibroin, cellulose and chitin) are easy to process, and have adaptable performance, which makes them have potential in organic, electrical or ionic conductivities by combining with highly conductive materials or changing their structure through chemical modification.[4–9] Among them, the cellulose-based flexible film builds a bridge between natural biomaterials and flexible bioelectronics due to its outstanding mechanical, flexible and adaptable conductive properties. As a carrier material or a framework support material, the properties of the cellulose-based flexible film can be changed and expanded by *in situ* polymerization or in combination with conductive materials. For example, cellulose-based flexible films can be combined with carbon nanotubes or graphene for flexible electrodes,[10,11] combined with metal oxides for photovoltaic materials and solar cells,[12,13] and combined with conductive polymers for electrochemical sensors.[14–16]

The manufacturing process of cellulose-based flexible films usually includes multiple steps, including the use of chemical, mechanical, or biological methods to decompose cellulose fibers, dispersing cellulose fibers in a solution, and restructuring through a bottom-up method.[17–20] Although the bottom-up method can achieve fine control of the film structure, the cost of the multi-step manufacturing process is relatively high, and the manufacturing yield is low, which makes it a less competitive method in scalable applications. In this context, a low-cost, scalable, simple and effective manufacturing method is ideal, but it also poses a challenge to the design.

Here, we show a simple top-down method to construct a cellulose-based flexible film (CF) that can be compounded with conductive materials directly from cellulose-based natural wood. First, treat natural wood (NW) with deep eutectic solvent (DES) to obtain treated CF. CF shows a unique 3D porous structure, with many channels, and excellent flexibility caused by the removal of part of lignin/hemicellulose by DES (Fig. 1). In recent years, DES has been widely used in the preparation of cellulosic materials,[21–24] which is a low-temperature eutectic mixture composed of hydrogen bond acceptors (such as quaternary ammonium salts) and hydrogen bond donors (such as carboxylic acids, polyols) in a certain molar ratio; its synthesis requires simple mixing and stirring of the components, no other purification treatment is required.[25–27] Compared with the common treatment method of removed wood lignin/hemicellulose by used a mixed alkaline solution of Na_2SO_3 or $NaClO_2$ and NaOH, the treatment process of DES is more gentle, and it is inexpensive, green and environmentally friendly, and will not produce toxic gases in the experiment. In the following specific experiments, we chose carbon nanotubes (CNTs) as the conductive material composited with CF, and

[a]*College of Furnishings and Industrial Design, Nanjing Forestry University, Nanjing 210037, Jiangsu, China. E-mail: wuyan@njfu.edu.cn*

[b]*Co-Innovation Center of Efficient Processing and Utilization of Forest Resources, Nanjing Forestry University, Nanjing 210037, China*

[c]*Fashion Accessory Art and Engineering College, Beijing Institute of Fashion Technology, Beijing, China. E-mail: yangfeng@bift.edu.cn*

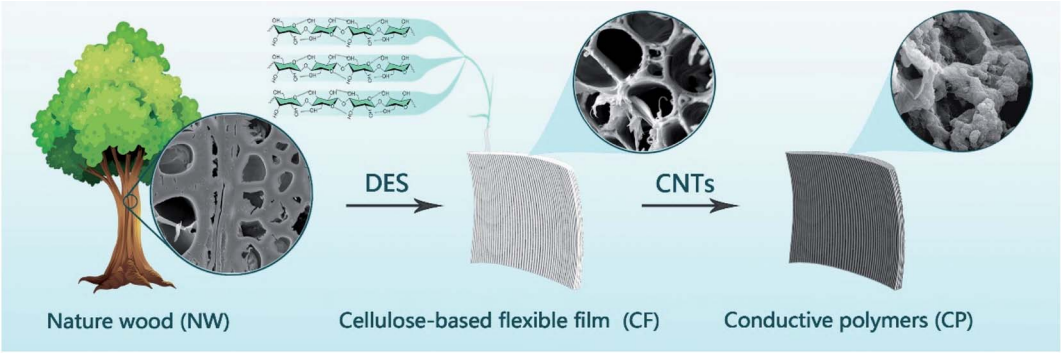

Fig. 1 Graphic illustration of the conductive polymers made from natural wood.

through the vacuum pressure impregnation technology to infiltrate carbon nanotubes (CNTs) into the CF to obtain cellulose-based conductive polymer (CP). CNTs have huge application potential in the development of basic electrochemical and (bio)electronic devices because of their unique structure, electrical and mechanical properties.[28–30] CP synthesized by CF and CNTs has excellent flexibility and certain conductivity, and shows good sensing ability under a certain range of strain/stress and human activity conditions.

2. Experimental section

Materials and chemicals

Ash wood (Fraxinus spp) was used for the fabrication of conductive polymer, its density was about 0.68 g cm^{-3}, provided by Yihua Life Technology Co., Ltd. (Shantou, China). The choline chloride as the hydrogen bond acceptor in the experiment was purchased from Sinopharm Chemical Reagent Co., Ltd., China; lactic acid as a hydrogen bond donor was provided by Shanghai Aladdin Biochemical Technology Co., Ltd., China; hydrogen peroxide solution was obtained from Shanghai Macklin Biochemical Co., Ltd., China; ethanol was purchased from Nanjing Chemical Reagent Co., Ltd., China; and carbon nanotubes (OD: 20–30 nm; ID: 5–10 nm; length: 10–30 μm) was obtained from Jiangsu Xianfeng Nano Material Technology Co., Ltd., China. All of the chemicals used were of analytical grade.

Treatment process for cellulose-based flexible film

First, the nature wood sample was dried in an oven at 102 °C for 6 hours, and then the dried sample was immersed in an absolute ethanol solution for 3 hours under vacuum. The wood dipped in absolute ethanol is immersed in DES (lactic acid and choline chloride are mixed at a molar ratio of 10 : 1), and heated at a high temperature of 90 °C for 5 hours. Then the sample in DES was taken out for microwave treatment, the microwave power was 600 W, and the duration of each microwave treatment was 20 s, repeated three times. After the microwave treatment, the above-mentioned sample was put into the DES again and heated at a high temperature of 80 °C for 2 hours. Because the DES solution was easy to darken the color of the sample, hydrogen peroxide solution was selected to bleach the sample. After bleaching was completed, the sample needs to be immersed in boiling deionized water several times to remove chemical substances to obtain a cellulose-based flexible film.

The preparation process of conductive polymer

The carbon nanotubes were dispersed in water by sonication to obtain a 0.5 wt% carbon nanotube suspension. Then the cellulose-based flexible film was immersed in a suspension of carbon nanotubes and heated under pressure at 8 MPa and 90 °C for 12 hours in a vacuum oven, so that the carbon nanotubes can fully penetrate into the cellulose-based flexible film. Finally, the cellulose-based flexible film loaded with carbon nanotubes was dried to obtain a conductive polymer.

Measurements and characterization

A FEI Quanta 200 scanning electron microscope (SEM) equipped with an energy dispersive X-ray spectroscopic detector for mapping were used to observe the morphology and structure of the sample under an accelerating voltage of 30 kV. The Fourier transform infrared spectrometer (VERTEX 80V, from Bruker Co., Ltd., Germany) was used to measure the FT-IR spectrum. The cellulose, hemicellulose, and lignin contents of the samples were tested by the Laboratory Analytical Procedure (LAP) written by the National Renewable Energy Laboratory (Determination of Structural Carbohydrates and Lignin in Biomass).[31] The lignin content was measured by two-step sulfuric acid hydrolysis, and the sugar content was analyzed by high-performance liquid chromatography (HPLC). The ASAP2020 automatic specific surface area and pore size distribution meter (from Micromeritics Co., Ltd., USA) was used to measure the BET surface area and adsorption average pore width. The conductivity of CP was recorded by RTS-9 double-electricity four-probe tester. A Keithley 2400 Source Meter was used to supply a current between the two farthest electrodes, and a Keithley 2182A nanovoltmeter was used to measure a voltage between the two intermediate electrodes. The resistance change was recorded in real time by DMM7510 digital graphic sampling multimeter (from Keithley Instruments Co., Ltd., USA); the test conditions were room temperature 20 °C, humidity 30–35%, and the test voltage was 1 V. XRD was measured on a Rigaku Ultima IV equipped with a curved detector manufactured by Rigaku

Americas Corp. The mechanical performance of the samples was evaluated using a universal testing machine (AG-IC 100KN, from SHIADAZU Co., Ltd., Japan).

3. Results and discussion

As a natural biological material, wood is one of the most abundant resources on earth. The lignocellulose component gives wood a unique three-dimensional porous structure, including vertically arranged microchannels and oriented cellulose nanofibers. However, natural wood is hard and fragile in nature and has poor flexibility. After the natural wood film was treated with DES, its flexibility had significantly enhanced. As shown in Fig. 2a and b, natural wood film was easily broken when bent, while CF will not break even when severely folded and twisted. The three-dimensional porous structure of wood has the complexity of combining micro, medium and large pores, which determines the flexibility of wood to a certain extent.[32] In order to further understand the microstructure characteristics of NW and CF, we carried out scanning electron microscopy (SEM) tests to compare the changes in wood cell structure before and after chemical treatment. The SEM results showed that after DES treatment, the pores inside the CF were preserved but some changes occurred in the morphology. As shown in Fig. 2c and d, the cell cavity of NW is small and the cell wall is thick, while the cell wall of CF is larger, and the cell wall becomes thinner. Meanwhile, CF creates more micro-scale pores in the corners of the cell wall rich in lignin, showing a porous structure, but NW cells did not show this situation.

In order to further understand the chemical structure change of CF compared with NW after DES treatment, we have carried out various measurements, including the main chemical composition of wood, Fourier transform infrared spectroscopy (FT-IR), X-ray diffraction (XRD) and BET surface area and adsorption average pore size, in order to explain the flexibility of CF from the chemical structure level. The cellular structure of wood is mainly composed of cellulose, hemicellulose and lignin, which are entangled with each other to provide the necessary mechanical integrity for the wood.[33] Fig. 3a shows the determination of cellulose, hemicellulose and lignin content before and after NW chemical treatment, which shows that DES significantly removed part of hemicellulose and a considerable amount of lignin. This is because DES provides a mild acid–base catalytic mechanism in the chemical treatment process, which can selectively break unstable ether bonds between phenylpropane units, depolymerize lignin/hemicellulose and separate it from biomass. The FTIR spectra of NW and CF also proved this point. As shown in Fig. 3b, the chemical treatment significantly reduces the groups of lignin and hemicellulose, and the characteristic lignin peaks are at 1593, 1505 and 1462 cm^{-1} (aromatic skeletal vibrations) almost disappeared, and the intensity of the hemicellulose related peaks at 1736 and 1235 cm^{-1} was significantly reduced.[34,35] The removal of lignin/hemicellulose allows the porosity of the wood to be increased without changing the cellulose crystal structure, which can be confirmed by the XRD patterns of NW and CF that are not much different (Fig. 3d). On the other hand, the average pore width based on BET adsorption indicates that delignification makes the wood produce more nano-pores with smaller pore widths (Fig. 3c), which may be caused by the removal of lignin and the collapse or shrinkage of cell walls. Meanwhile, the results of the BET test showed that the surface area of the wood after delignification increased from 0.92 $m^2 g^{-1}$ to 1.57 $m^2 g^{-1}$, this well-developed porous structure is not only conducive to the flexibility of CF, but also conducive to the subsequent penetration of carbon nanotubes (Fig. 3c).

Due to the removal of partial hemicellulose and lignin, CF has obtained a more porous structure, which facilitates the

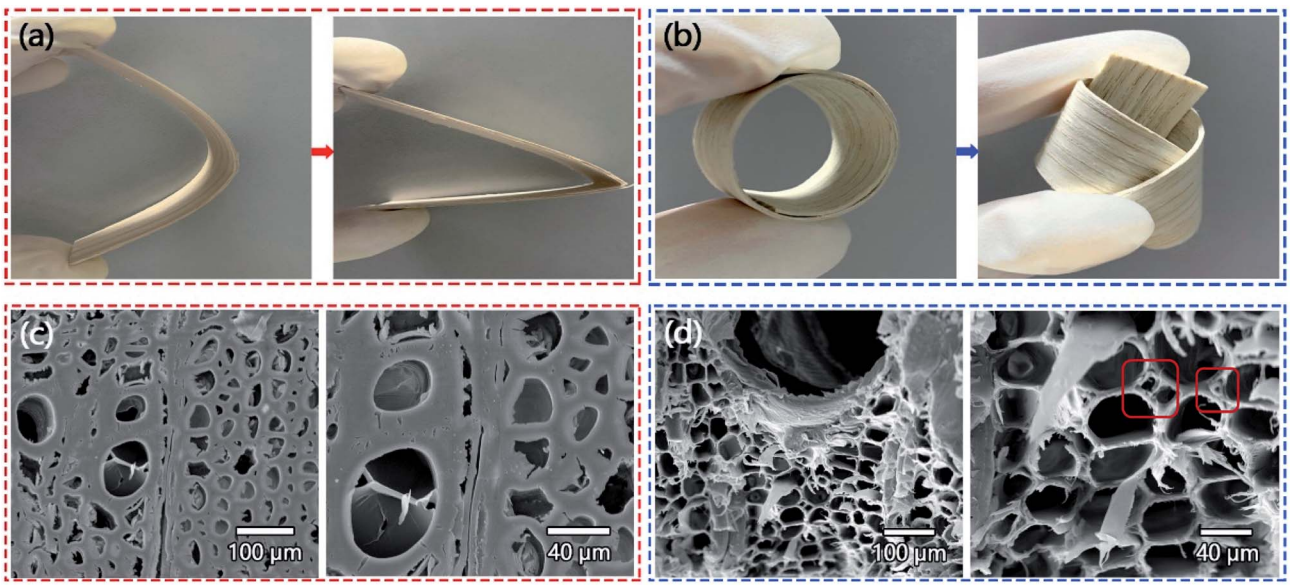

Fig. 2 Comparison of flexibility and microscopic appearance of the NW and CF. (a) NW breaks upon bending. (b) CF becomes highly flexible upon bending. (c) SEM image of NW at cross sections. (d) Cross-sectional SEM image of CF to show the porous structures.

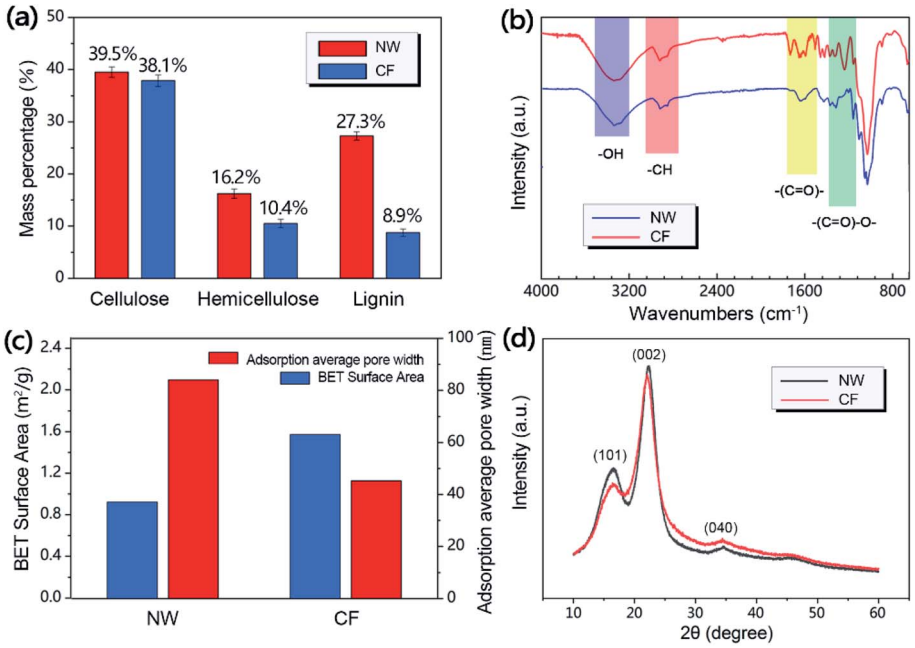

Fig. 3 Characterization of the chemical structure of NW and CF. (a) Content evolutions of cellulose, hemicellulose and lignin in NW and CF. (b) FTIR spectra of NW and CF. (c) BET surface area and adsorption average pore width of NW and CF. (d) XRD patterns of the NW and CF.

successful introduction of CNTs into the wood cell cavity by vacuum pressure impregnation to obtain CP. Cellulose-based wood cells (axial vessels) have a cylindrical structure, mainly running parallel to the trunk, forming a continuous porous network that transports water and nutrients.[36] Therefore, these pre-existing microchannel networks can be used for the infiltration and alignment of foreign CNTs to achieve continuous conduction. After the vacuum pressure impregnation treatment, CP obtained the black coating as shown in Fig. 4a and extended into the internal structure of the wood, which was confirmed by the scanning electron microscope (SEM) image of the lateral structure of CP. As shown in Fig. 4b and c, in the cross section of the CP, it can be observed that the nanoparticles filled the internal pore structure of the wood. Through further magnification of the SEM image, it can be determined that the nanoparticles in the internal pores of the wood are CNTs (Fig. 4d and e). It is worth noting that the occupation of the wood microchannel network by CNTs and the processing methods of VPI did not cause visible damage to the cellulose skeleton structure of CP, and CP can maintain structural stability while possessed a certain degree of conductivity.

In order to further study the conductivity of CP, the RTS-9 double-electricity four-probe machine was used to test the conductivity of CF and CP. In order to reduce the error of the experiment, five different points are taken during the test of each sample, and the final result is the average value. The results show that CP loaded with CNTs has a high conductivity of 0.94 s cm^{-1}, while CF has no conductivity (Fig. 5a). Fig. 5b shows the digital images of the CP slices connected in series with the light-emitting diodes, it can be found that the CP lighted up the light-emitting diode bulbs, which proves the good conductivity of the CP. The good conductivity of CP is due to the composite of CNTs and CF. The relative element content of CF and CP was determined by energy dispersive X-ray spectroscopy, it was found that the C element content of CP was 54.5 wt%, while the carbon content of CP was as high as 70.3 wt%. The change of C element content was caused by the introduction of CNTs by CF. Moreover, CP inherits the vertically arranged microchannels and oriented cellulose nanofiber structure of CF, which allows us to prepare conductive fibers by cutting and twisting the oriented cellulose nanofibers (Fig. 5e and f),[37,38] and the obtained conductive fibers can light up diode bulbs just like CP (Fig. 5c). As an extended application of CP, conductive fibers have certain potential in the field of wearable electronic devices.[39]

Good mechanical properties are crucial to the practical application of CP, so CP was further evaluated by mechanical tensile test. Fig. 6a shows the representative stress–strain curves of NW, CF and CP, it can be seen that CF and CP can produce higher strains at fractured than NW, but the tensile stress that CF can withstand was lower than that of NW and CP, and CP has the highest tensile strength. Because CF was treated with DES to remove part of the lignin/hemicellulose, the pores of the cellulose-based wood are increased, and a flexible porous network structure was formed, which the structure allows the CF to produce greater deformation without breaking when being stretched.[40] CP prepared on the basis of CF inherits this characteristic, and the strain produced at fractured was only 5% lower than that of CF. While producing larger strain, CP can also withstand larger tensile stress and obtain higher tensile strength (94.8 MPa). As a polymer of CF and CNTs, CP has a denser structure than CF. CNTs are interspersed in the structure of cellulose-based wood structure and play a certain mechanical support for wood cell walls; on the other hand, due

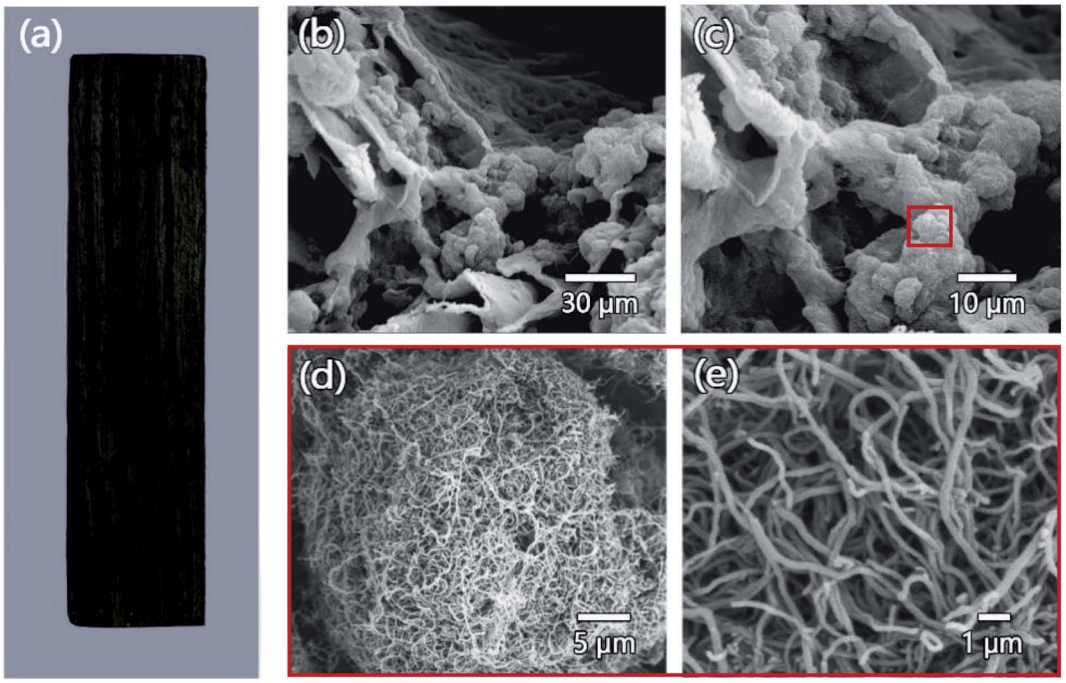

Fig. 4 Microstructure characterization of CP. (a) Digital image of CP. (b) Cross-sectional SEM image of CP. Many CNTs are distributed in the wood cell cavity. (c) The high magnification SEM image of the CP cross section to show CNTs. (d) SEM image of CNTs. (e) High magnification SEM image of CNTs to show the morphology of CNTs.

to the small size of the CNTs particles and the large specific surface area, there is a strong van der Waals force between the tubes, which consumes more energy during the stretching process, resulting in higher mechanical tensile strength.[41] In addition, the higher tensile strength and tensile strain of CP resulted in the CP obtaining a toughness of 5.48 MJ m^{-3}, which

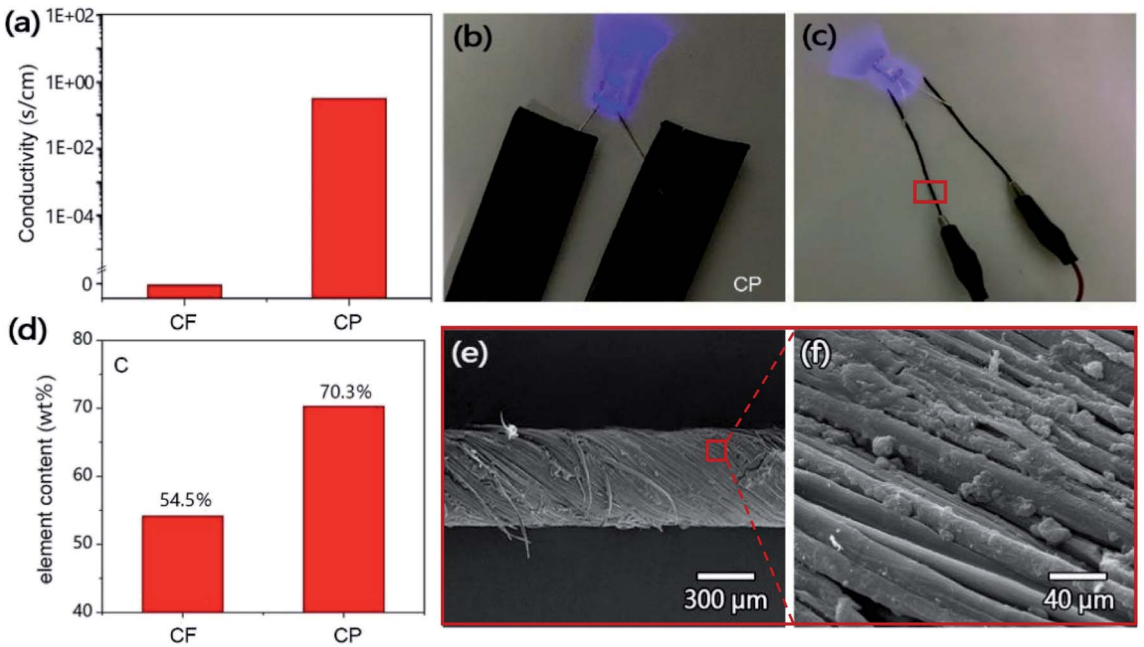

Fig. 5 Electrical conductivity of CP. (a) Electrical conductivity of CF and CP. (b and c) Digital image to demonstrate the CP and conductive fiber can light up a LED bulb. (c) The digital image shows that the conductive fiber lighted up the LED bulb. (d) Relative element content of carbon in CF and CP, which was obtained from the results of energy dispersive X-ray spectroscopy. (e) Lateral surface SEM image of the conductive fiber, which was made by cutting and twisted the CP. (f) A high-magnification SEM image of the side of the conductive fiber lateral surface.

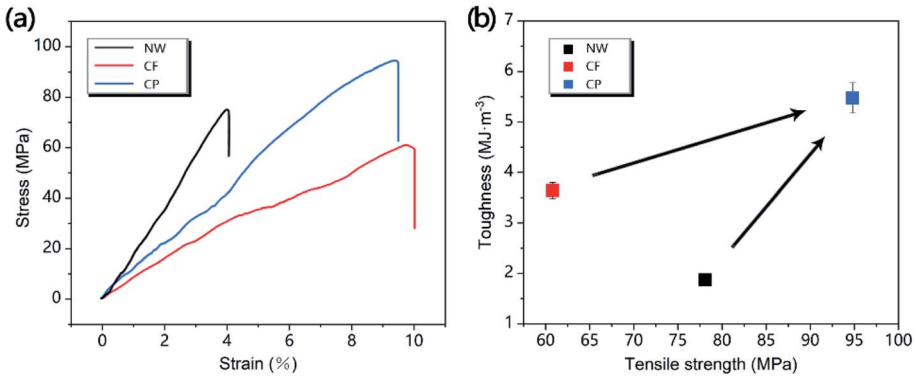

Fig. 6 Comparison of mechanical properties of NW, CF and CP. (a) Representative stress–strain curves of NW, CF and CP. (b) Relationship of toughness and tensile strength for NW, CF and CP.

was nearly 3 times that of NW (1.87 MJ m^{-3}) and 1.5 times that of CF (3.64 MJ m^{-3}) (Fig. 6b). The good toughness of CP provides an important guarantee for its application in flexible electronic devices, smart wearable devices and other fields.

CP has broad application prospects in the field of flexible electronic devices, including memory devices,[42] pressure sensors,[43] and artificial electronic skins.[44,45] Here, the CP's ability to sense strain/stress was preliminarily studied. Fig. 7a and b show the correlation between the resistance change of CP and mechanical strain/stress. With the cycle of strain/stress, the relative resistance of CP also shows a monotonic linear cycle, showing linear resistance characteristics within the strain/stress range studied.[46] Fig. 7a shows the resistance change curve of CP at different strains of 3% and 7%. Under the lower strain cycle (3% strain), the resistance change signal of CP was sharp, uniform and reversible. When the strain cycle value approaches the maximum strain of CP (9.48% strain), the peak value of the resistance change curve begins to increase gradually (Fig. 7a), which may be caused by a small amount of unrecoverable deformation caused by multiple stretches. Moreover, the resistance change measurement performed in 10 stress cycles proves that the electrical signal of CP in the sensing process has very good repeatability (Fig. 7b), so CP has great potential as a strain/stress sensor. Based on this point of view, we explored the potential application of CP in human activity recognition. Fig. 7c shows the practical application of CP as a physiological sensing platform. It was attached to a human finger and then sealed with a transparent tape to monitor the resistance change caused by human motion strain. The results show that the sensor can quickly switch between loading and unloading, the resistance changes of human movement were accurately recorded, and its signal response was repeatable and stable. Therefore, CP also has bright application prospects as a high-sensitivity monitor for identifying human activities.

4. Conclusions

In summary, we have shown an effective way to directly construct a cellulose-based flexible film that can be compounded with conductive materials from cellulose-based natural wood. Using natural wood as a starting material, a cellulose-based flexible film with a porous structure can be obtained through DES treatment, and this porous structure facilitates the subsequent penetration of carbon nanotubes to obtain conductive polymers. This is a low-cost, high-efficiency, and non-toxic process, which provides a new idea for the preparation of conductive composite materials. The research results show that the combination of carbon nanotubes and cellulose-based flexible films not only brings high conductivity of up to 0.94 s cm^{-1} to the material, but also exhibits amazing

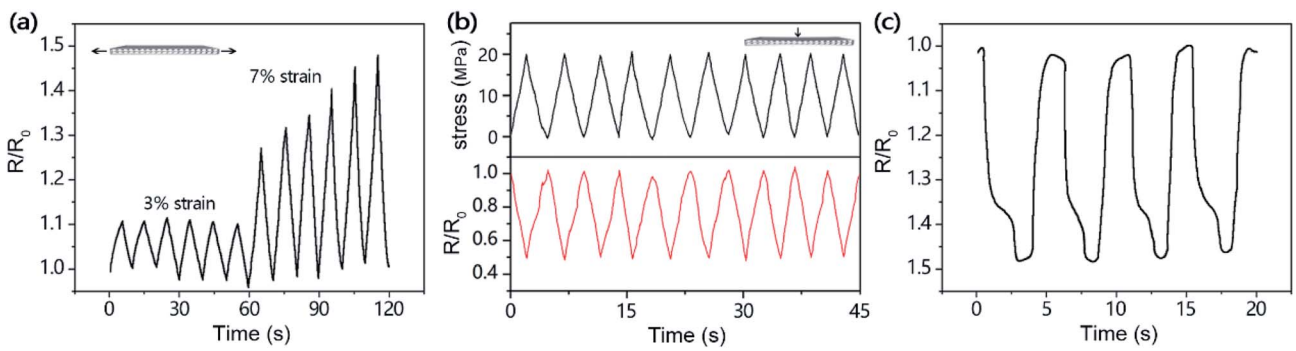

Fig. 7 Strain/stress and touch sensing behavior of CP. (a) Resistance change of CP in different strains (3 and 7%) (b) resistance changes of CP in 10 stress cycles. (c) The changing resistance of the CP corresponds to the strain change of finger bending.

functional perception to external stimuli. Within a certain strain/stress range, the electrical signal of this conductive polymer has very good repeatability and stability. In addition, conductive fibers can be prepared by cutting and twisting the oriented cellulose nanofibers of this conductive polymer. This simple, top-down method can easily prepare cellulose-based conductive polymers, which is expected to open up a series of new possibilities in flexible electronic devices, tactile sensor, and other fields.

Funding

The authors gratefully acknowledge the financial support from the project funded by the National Natural Science Foundation of China (32071687 and 32001382), the Project of Science and Technology Plan of Beijing Municipal Education Commission (KM202010012001).

Conflicts of interest

The authors declare no competing financial interest.

Acknowledgements

The authors gratefully acknowledgment the financial support from the Peoples' Republic of China.

References

1 M. Teodorescu, M. Bercea and S. Morariu, *Polym. Rev.*, 2018, **58**, 247–287.
2 K. Joyce, G. T. Fabra, Y. Bozkurt and A. Pandit, *Signal Transduction Targeted Ther.*, 2021, **6**, 1–28.
3 H. Samadian, H. Maleki, Z. Allahyari and M. Jaymand, *Coord. Chem. Rev.*, 2020, **420**, 213432.
4 C. Zhang, Y. Zhang, H. Shao and X. Hu, *ACS Appl. Mater. Interfaces*, 2016, **8**, 3349–3358.
5 W. Liu, Z. Zhou, S. Zhang, Z. Shi, J. Tabarini, W. Lee, Y. Zhang, S. N. Gilbert Corder, X. Li, F. Dong, L. Cheng, M. Liu, D. L. Kaplan, F. G. Omenetto, G. Zhang, Y. Mao and T. H. Tao, *Adv. Sci.*, 2017, **4**, 1700191.
6 X. Wang, C. Yao, F. Wang and Z. Li, *Small*, 2017, **13**, 1702240.
7 D. Zhao, Y. Zhu, W. Cheng, W. Chen, Y. Wu and H. Yu, *Adv. Mater.*, 2020, **14**, 2000619.
8 K. Kim, M. Ha, B. Choi, S. H. Joo, H. S. Kang, J. H. Park, B. Gu, C. Park, C. Park, J. Kim, S. K. Kwak, H. Ko, J. Jin and S. J. Kang, *Nano Energy*, 2018, **48**, 275–283.
9 M. G. Casteleijn, D. Richardson, P. Parkkila, N. Granqvist, A. Urtti and T. Viitala, *Colloids Surf., A*, 2018, **539**, 261–272.
10 M. M. Pérez-Madrigal, M. G. Edo and C. Alemán, *Green Chem.*, 2016, **18**, 5930–5956.
11 H. Luo, J. Xie, L. Xiong, Y. Zhu, Z. Yang and Y. Wan, *Composites, Part B*, 2019, **162**, 484–490.
12 S. Cao, X. Feng, Y. Song, H. Liu, M. Miao, J. Fang and L. Shi, *ACS Appl. Mater. Interfaces*, 2016, **8**, 1073–1079.
13 Q. Cheng, D. Ye, W. Yang, S. Zhang, H. Chen, C. Chang and L. Zhang, *ACS Sustainable Chem. Eng.*, 2018, **6**, 8040–8047.
14 D. B. K. Lim and H. Gong, *Carbohydr. Polym.*, 2018, **201**, 446–453.
15 Q. Fu, Y. Chen and M. Sorieul, *ACS Appl. Mater. Interfaces*, 2020, **14**, 3528–3538.
16 Y. Wang, L. Zhang, J. Zhou and A. Lu, *ACS Appl. Mater. Interfaces*, 2020, **12**, 7631–7638.
17 K. M. O. Håkansson, A. B. Fall, F. Lundell, S. Yu, C. Krywka, S. V. Roth, G. Santoro, M. Kvick, L. Prahl Wittberg, L. Wågberg and L. D. Söderberg, *Nat. Commun.*, 2014, **5**, 4018.
18 N. Mittal, F. Ansari, V. Gowda Krishne, C. Brouzet, P. Chen, P. T. Larsson, S. V. Roth, F. Lundell, L. Wågberg, N. A. Kotov and L. D. Söderberg, *ACS Nano*, 2018, **12**, 6378–6388.
19 H. Sehaqui, N. Ezekiel Mushi, S. Morimune, M. Salajkova, T. Nishino and L. A. Berglund, *ACS Appl. Mater. Interfaces*, 2012, **4**, 1043–1049.
20 H. Tang, N. Butchosa and Q. Zhou, *Adv. Mater.*, 2015, **27**, 2070–2076.
21 J. A. Sirviö, M. Visanko and H. Liimatainen, *Green Chem.*, 2015, **17**, 3401–3406.
22 Y. Chen and T. Mu, *Green Energy Environ.*, 2019, **4**, 95–115.
23 J. A. Sirviö, *J. Mater. Chem. A*, 2019, **7**, 755–763.
24 J. A. Sirviö, K. Hyypiö, S. Asaadi, K. Junka and H. Liimatainen, *Green Chem.*, 2020, **22**, 1763–1775.
25 H. Malaeke, M. R. Housaindokht, H. Monhemi and M. Izadyar, *J. Mol. Liq.*, 2018, **263**, 193–199.
26 S. Hong, X. J. Shen, B. Pang, Z. Xue, X. F. Cao, J. L. Wen, Z. H. Sun, S. S. Lam, T. Q. Yuan and R. C. Sun, *Green Chem.*, 2020, **22**, 1851–1858.
27 R. Yang, Q. Cao, Y. Liang, S. Hong, C. Xia, Y. Wu, J. Li, L. Cai, C. Sonne, Q. Van Le and S. S. Lam, *Chem. Eng. J.*, 2020, **401**, 126150.
28 M. Chen, X. Qin and G. Zeng, *Trends Biotechnol.*, 2017, **35**, 836–846.
29 I. A. Kinloch, J. Suhr, J. Lou, R. J. Young and P. M. Ajayan, *Science*, 2018, **362**, 547–553.
30 X. Wang, A. Dong, Y. Hu, J. Qian and S. Huang, *Chem. Commun.*, 2020, **56**, 10809–10823.
31 A. Sluiter, B. Hames, R. O. Ruiz, C. Scarlata, J. Sluiter and D. Templeton, *Technical Report NREL/TP-510-42618*, National Renewable Energy Laboratory: Golden, CO, DOI: 10.1007/s00449-014-1243-0.
32 Q. Xia, C. Chen, Y. Yao, S. He, X. Wang, J. Li, J. Gao, W. Gan, B. Jiang, M. Cui and L. Hu, *Adv. Mater.*, 2021, **20**, 2001588.
33 Y. Wu, J. Zhou, Q. Huang, F. Yang, Y. Wang, X. Liang and J. Li, *ACS Omega*, 2020, **5**, 1782–1788.
34 J. Wu, Y. Wu, F. Yang, C. Tang, Q. Huang and J. Zhang, *Composites, Part A*, 2019, **117**, 324–331.
35 C. Huang, Y. Su, J. Shi, C. Yuan, S. Zhai and Q. Yong, *New J. Chem.*, 2019, **43**, 3520–3528.
36 V. Merk, M. Chanana, N. Gierlinger, A. M. Hirt and I. Burgert, *ACS Appl. Mater. Interfaces*, 2014, **6**, 9760–9767.
37 X. Yang and L. A. Berglund, *Adv. Mater.*, 2020, **20**, 2001118.
38 K. Abe and M. Utsumi, *Cellulose*, 2020, **27**, 10441–10446.
39 Z. Yang, Z. Zhai, Z. Song, Y. Wu, J. Liang, Y. Shan, J. Zheng, H. Liang and H. Jiang, *Adv. Mater.*, 2020, **32**, 1907495.

40 Y. Wu, L. Yang, J. Zhou, F. Yang, Q. Huang and Y. Cai, *ACS Omega*, 2020, **5**, 22163–22170.
41 D. G. Papageorgiou, Z. Li, M. Liu, I. A. Kinloch and R. J. Young, *Nanoscale*, 2020, **12**, 2228–2267.
42 T. Liu, W. Wu, K. N. Liao, Q. Sun, X. Gong, V. A. L. Roy, Z. Z. Yu and R. K. Y. Li, *Carbohydr. Polym.*, 2019, **214**, 213–220.
43 X. Zhou, L. Zhu, L. Fan, H. Deng and Q. Fu, *ACS Appl. Mater. Interfaces*, 2018, **10**, 31655–31663.
44 Z. He, W. Chen, B. Liang, C. Liu, L. Yang, D. Lu, Z. Mo, H. Zhu, Z. Tang and X. Gui, *ACS Appl. Mater. Interfaces*, 2018, **10**, 12816–12823.
45 J. Ge, L. Sun, F. R. Zhang, Y. Zhang, L. A. Shi, H. Y. Zhao, H. W. Zhu, H. L. Jiang and S. H. Yu, *Adv. Mater.*, 2016, **28**, 722–728.
46 L. Li, X. Fu, S. Chen, S. Uzun, A. S. Levitt, C. E. Shuck, W. Han and Y. Gogotsi, *ACS Appl. Mater. Interfaces*, 2020, **12**, 15362–15369.